PROCEEDINGS OF SPIE

SPIEDigitalLibrary.org/conference-proceedings-of-spie

Ultrafast and highly efficient resonant-cavity-enhanced photodiodes

Ekmel Ozbay
Ibrahim Kimukin
Necmi Biyikli

SPIE.

Downloaded From: https://www.spiedigitallibrary.org/conference-proceedings-of-spie on 9/28/2017 Terms of Use: https://spiedigitallibrary.spie.org/ss/TermsOfUse.aspx

Ultrafast and highly efficient resonant cavity enhanced photodiodes

Ekmel Özbay[a], İbrahim Kimukin[a], Necmi Bıyıklı[b]

[a]Department of Physics, Bilkent University, 06800 Ankara, TURKEY
[b]Department of Electrical and Electronics Engineering, Bilkent University, 06800 Ankara, TURKEY

ABSTRACT

In this talk, we will review our research efforts on resonant cavity enhanced (RCE) high-speed high-efficiency photodiodes (PDs) operating in the 1st and 3rd optical communication windows. Using a microwave compatible planar fabrication process, we have designed and fabricated GaAs and InGaAs based RCE photodiodes. For RCE GaAs Schottky type photodiodes, we have achieved peak quantum efficiencies of 50% and 75% with semi-transparent (Au) and transparent (indium-tin-oxide) Schottky layers respectively. Along with 3-dB bandwidths of 50 and 60 GHz, these devices exhibit bandwidth-efficiency (BWE) products of 25 GHz and 45 GHz respectively. By using a postprocess recess etch, we tuned the resonance wavelength of an RCE InGaAs PD from 1605 to 1558 nm while keeping the peak efficiencies above 60%. The maximum quantum efficiency was 66% at 1572 nm which was in good agreement with our theoretical calculations. The photodiode had a linear response up to 6 mW optical power, where we obtained 5 mA photocurrent at 3 V reverse bias. The photodetector had a temporal response of 16 psec at 7 V bias. After system response deconvolution, the 3-dB bandwidth of the device was 31 GHz, which corresponds to a bandwidth-efficiency product of 20 GHz.

Keywords: High-speed photodetectors, resonant cavity enhancement, Schottky diode, p-i-n photodiode, quantum efficiency, bandwidth-efficiency product.

1. INTRODUCTION

As the information revolution continues at an increasing pace, there is an exponentially increasing demand for larger telecommunication bandwidths. The optical communication systems are currently the only viable solution for this bandwidth demand. Optoelectronic components such as semiconductor lasers, photodetectors, modulators, and optical amplifiers are at the heart of these communication systems, and the performance of all these devices should be increased to meet the existing and expected bandwidth requirements. Besides the optical communication systems, high-performance photodetectors are also vital components of optical measurement systems [1-3]. Both Schottky PDs, [4-6] and p-i-n PDs, [7,8] offer high-speed performance to fulfill the needs of such systems. However, the efficiency of these detectors has been typically limited to less than 10%, mostly due to the thin absorption region needed for short transit times. One can increase the absorption region thickness to achieve higher efficiencies, but this also means longer transit times that will degrade the high-speed performance of the devices. One detection scheme to overcome this limitation is edge-coupled photodiodes. This scheme has been used to achieve very high-speed metal-semiconductor-metal (MSM) or p-i-n waveguide photodiodes distributed MSM photodetectors, avalanche photodiodes, and traveling-wave photodetectors with high output current [9-13]. The disadvantages of edge-illuminated detectors are complex fabrication and integration along with difficult light coupling.

RCE photodetectors offer the possibility of overcoming this limitation in the BWE product of conventional PDs [14-16]. The ease of fabrication, integration, and optical coupling makes the resonant cavity enhanced (RCE) PDs attractive for high-performance photodetection [17-20]. High-speed RCE photodetector research has mainly concentrated on using p-i-n PDs [25] and avalanche PDs, where 35 GHz low-gain bandwidth [26], and 17 GHz BWE performance [27] have been reported. In our work, we have fabricated RCE Au-Schottky PDs with 50% quantum efficiency and a 50 GHz frequency performance [28]. Recently, we have improved the performance of RCE Schottky type PDs to 60 GHz bandwidth, along with a 75% quantum efficiency via a transparent Schottky layer and top dielectric Bragg mirror [29]. For the InGaAs based p-i-n type RCE PDs we achieved 66% quantum efficiency along with a 31 GHz performance [30]. In this paper, we review our recent work on design, fabrication, and characterization of high performance RCE PDs.

Active and Passive Optical Components for WDM Communications III, Achyut K. Dutta, Abdul Ahad S. Awwal, Niloy K. Dutta, Kazuo Fujiura, Proceedings of SPIE Vol. 5246 (2003)
© 2003 SPIE · 0277-786X/03/$15.00

Downloaded From: https://www.spiedigitallibrary.org/conference-proceedings-of-spie on 9/28/2017 Terms of Use: https://spiedigitallibrary.spie.org/ss/TermsOfUse.aspx

2. RESONANT CAVITY ENHANCEMENT

The well-known BWE trade-off is a major blockade for using high-speed PDs in long-haul telecommunications. As the active region thickness is decreased to minimize the transit time for high-speed purposes, the quantum efficiency of the same device proportionally decreases. For a PD with transit-time limited frequency response, the 3-dB bandwidth can be formulated as

$$f_{3dB} \approx 0.45\frac{v}{d}, \tag{1}$$

where ν is the drift velocity of the charge carrier, and d is the active region thickness. For thin active regions, the absorption can be formulated as

$$\eta = (1-R)(1-e^{-\alpha d}) \approx (1-R)\alpha d, \tag{2}$$

where α is the power absorption loss factor of the optical field within the active region, and αd <<1 is assumed. Using equations (1) and (2), the BWE product can be obtained as,

$$f_{3dB} \cdot \eta = 0.45(1-R)v\alpha, \tag{3}$$

which is independent of the active region thickness.

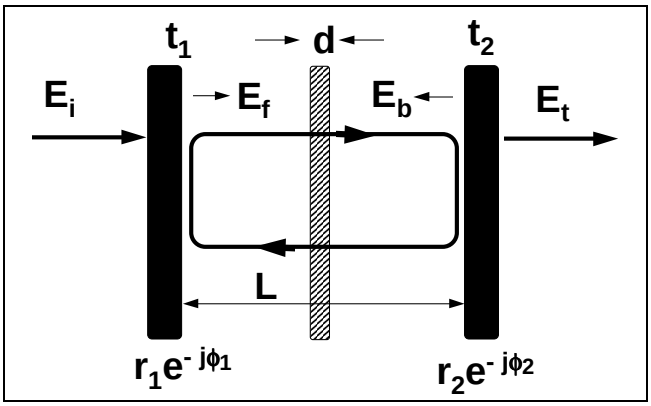

Figure 1. Schematics of the Fabry Perot cavity model. The shaded absorption region was used to simulate the active region placed in the cavity.

This BWE trade-off can be solved by placing the active region in a Fabry-Perot cavity (Fig.1). This is usually achieved by integrating the photoactive region with a bottom Bragg mirror. In a Fabry-Perot cavity, the optical field is enhanced resulting in increased efficiencies. The electric field component for the forward traveling wave E_f inside the cavity (Fig. 1) can be related to the incident field E_i as:

$$E_f = \frac{t_1}{1-r_1 r_2 e^{-\alpha d} e^{-j(2\beta L+\phi_1+\phi_2)}} E_i, \tag{4}$$

where $r_1e^{-j\phi 1}$ and $r_2e^{-j\phi 2}$ are the reflection coefficients of the mirrors, t_1 is the transmission coefficient of the front mirror,

Downloaded From: https://www.spiedigitallibrary.org/conference-proceedings-of-spie on 9/28/2017 Terms of Use: https://spiedigitallibrary.spie.org/ss/TermsOfUse.aspx

β is the propagation constant for the traveling EM wave in air, and L is the total width of the cavity. The backward traveling wave E_b is related to E_f as:

$$E_b = r_2 e^{-\alpha d} e^{-j(\beta L + \phi_2)} E_f \,. \tag{5}$$

Using equations (4) and (5), we can calculate the power enhancement factor η, which is defined as the ratio of the absorbed power inside the absorption layer, to the power of the incident EM wave,

$$\eta = \frac{(1 + R_2 e^{-\alpha d})(1 - R_1)}{1 - 2\sqrt{R_1 R_2} e^{-\alpha d} \cos(2\beta d + \phi_1 + \phi_2) + R_1 R_2 e^{-\alpha d}} \tag{6}$$

where $R_1 = r_1^2$ and $R_2 = r_2^2$, are the reflectivities of the mirrors of the cavity. The above result is normalized with respect to the incident field absorbed by the detector in the absence of the cavity. As can be seen from equation (6), the introduction of a Fabry-Perot cavity can increase the quantum efficiency without affecting the high-speed properties. Besides, the detector becomes wavelength selective, which may be very useful for wavelength division multiplexing (WDM) based optical communication systems.

The active layer thickness, d, was chosen such that the maximum quantum efficiency is obtained by,

$$R_1 = R_2 e^{-2\alpha d} \tag{7}$$

where α is the absorption coefficient, R_1 is the top air-semiconductor mirror reflectance, and R_2 is the bottom Bragg mirror reflectance [14].

3. GAAS BASED SCHOTTKY PHOTODETECTOR

3.1 Design and Fabrication

We've designed, fabricated and characterized RCE Schottky PDs with semi-transparent (thin Au metal) and transparent (indium-tin-oxide (ITO)) Schottky layers. Both diode structures were similarly designed using transfer-matrix-method (TMM) based theoretical simulations, except that the RCE Au-Schottky PD design had 18 pair bottom Bragg mirror whereas the RCE ITO-Schottky PD design had a bottom Bragg mirror of 24 pairs of $Al_{0.20}Ga_{0.80}As$/AlAs alternating $\lambda/4$-thick layers. A ~150 nm thick GaAs active layer was used in both designs, which was the only absorbing part of the detector cavity at the design wavelength of 820 nm. All the cavity layers, except the GaAs photo-absorption layer, were designed as $Al_{0.20}Ga_{0.80}As$, which is transparent at the operation wavelength. Therefore, no diffusion component of the photocurrent was expected in these heterostructure RCE-PD designs, which improves high-frequency performance of these devices.

The samples were fabricated using a microwave-compatible fabrication process. GaAs and AlGaAs layers were etched with an ammonia based etchent (HHO_3:H_2O_2:H_2O). First, ohmic contacts to the N+ layers were formed by a recess etch that was followed by a self-aligned Au-Ge-Ni liftoff. The samples were annealed at 450 ^{0}C. The Schottky contacts were achieved with either gold evaporation or ITO sputtering. Using an isolation mask, we etched away all of the epilayers, except the active areas. Then, we evaporated Ti/Au interconnect metal which formed coplanar waveguide (CPW) transmission lines on top of the semi-insulating substrate. The next step was the deposition and patterning of a 2000 Å thick silicon nitride layer. Finally, a 1.0 micron thick Au layer was used as an airbridge to connect the center of the CPW to the top Schottky metal.

3.2 Measurements

Downloaded From: https://www.spiedigitallibrary.org/conference-proceedings-of-spie on 9/28/2017 Terms of Use: https://spiedigitallibrary.spie.org/ss/TermsOfUse.aspx

3.2.1 Au-Schottky photodetectors

A thin (~10 nm) semitransparent Au film is deposited via thermal evaporation as the Schottky contact in these devices. As Schottky contact material, Au has excellent electrical properties and forms high-quality Schottky barriers with GaAs. The Au film also functions as the top mirror of the resonant cavity. However, it absorbs a significant portion of the incident light, thereby decreasing the efficiency of the detector. Moreover, the thin Au film has large surface fluctuations, which causes scattering of incident optical field. Fig. 2 shows the photoresponse of the fabricated RCE Au-Schottky PDs. The peak quantum efficiency is 50% around 827 nm under 2.5 V reverse bias. This value corresponds to a five-fold enhancement of the efficiency of a single-pass conventional PD with the same active layer thickness.

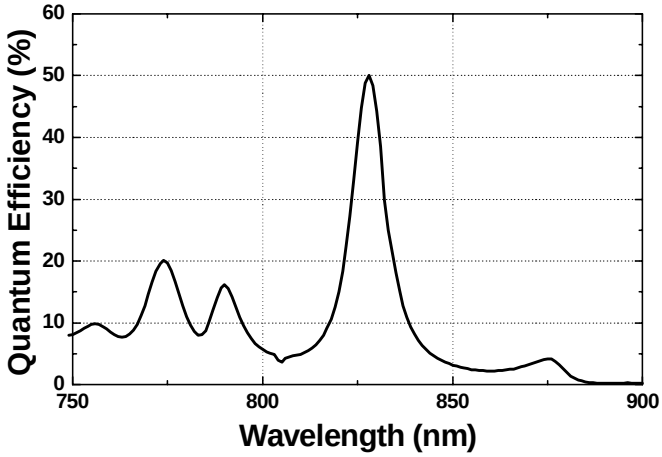

Figure 2. Spectral quantum efficiency measurement of Au-Schottky RCE photodetector

High-speed measurements were done using the similar high-frequency set-up described in the previous section. The best measured FWHM is 12 psec under 8 V reverse bias. Considering a 9 psec FWHM for the 50 GHz scope, the deconvolved pulse response has a 3-dB bandwidth of ~50 GHz. The detector response becomes considerably slower for reverse biases lower than 6 V. This observation indicates that a 6 V reverse bias is needed for full depletion of the absorbing GaAs layer, which is a result of the relatively high-doping in the depletion region.

3.2.2 ITO-Schottky photodetectors

ITO, which is known to be a transparent conductor, is a potential alternative to thin semi-transparent Au as the Schottky-contact material. Its transparency minimizes the problem of optical loss and scattering, resulting in higher efficiency performance [31,32]. However, due to its low refractive index ITO films show poor reflectivity. Therefore, for optimum RCE effect we need an additional top mirror.

The deposition of the Schottky-contact material ITO was done via RF magnetron sputtering in an Ar environment from a composite target containing by weight 90% In_2O_3 and 10% SnO_2. Before device fabrication, electrical and optical properties of sputtered thin ITO films were characterized. The resistivity of the as-grown ITO film was determined as $2x10^{-4}$ Ω-cm approximately. This value decreased to $1.5x10^{-4}$ Ω-cm and $1.2x10^{-4}$ Ω-cm when the films were annealed at 300 ^{o}C and 400 ^{o}C, respectively. Using a fiber-optic based optical transmission measurement set-up, the transmittivity of a 150 nm-thick ITO film deposited on a quartz substrate was measured. The transmittivity was around 87% at 820 nm, and increased very slightly (to ~88%) with annealing up to 450 ^{o}C. Reflectivity at the same wavelength was measured to be 12% before annealing, which indicated that the absorption in ITO film was ~1%. Another important optical property was the refractive index of the film, which was measured by an ellipsometer. The measured refractive index of the as-grown ITO film was 1.99, and this value decreased to 1.85 after the film was annealed at 450 ^{o}C.

Downloaded From: https://www.spiedigitallibrary.org/conference-proceedings-of-spie on 9/28/2017 Terms of Use: https://spiedigitallibrary.spie.org/ss/TermsOfUse.aspx

These results showed that the sputtered ITO films could be used as low-loss, high-quality Schottky contacts to our devices.

After the device fabrication is completed, the top mirror of the resonant cavity was formed by a PECVD-grown dielectric Si_3N_4/SiO_2 DBR centered at 820 nm. The resulting RCE-Schottky PDs had breakdown voltages around 8 V and typical dark current densities were $5x10^{-5}$ A/cm^2 at -1 V bias. By current-voltage measurements, the Schottky barrier height and the ideality factor of the ITO/GaAs Schottky contacts were determined as 0.74 eV and 1.12 respectively.

Fig. 3(a) shows the spectral quantum efficiency measurement of the RCE-Schottky PD without a dielectric top DBR mirror. The spectral quantum efficiency of the same device with a 2 pair Si_3N_4/SiO_2 top Bragg mirror is shown in Fig. 3(b). The peak quantum efficiency before top DBR deposition was 66% at 817 nm and increased to a maximum of 75% at 815 nm for a 2 pair top DBR mirror. Both measurements were done at zero bias. The peak quantum efficiency did not change with applied bias voltage, which indicated that the diode active layer was completely depleted.

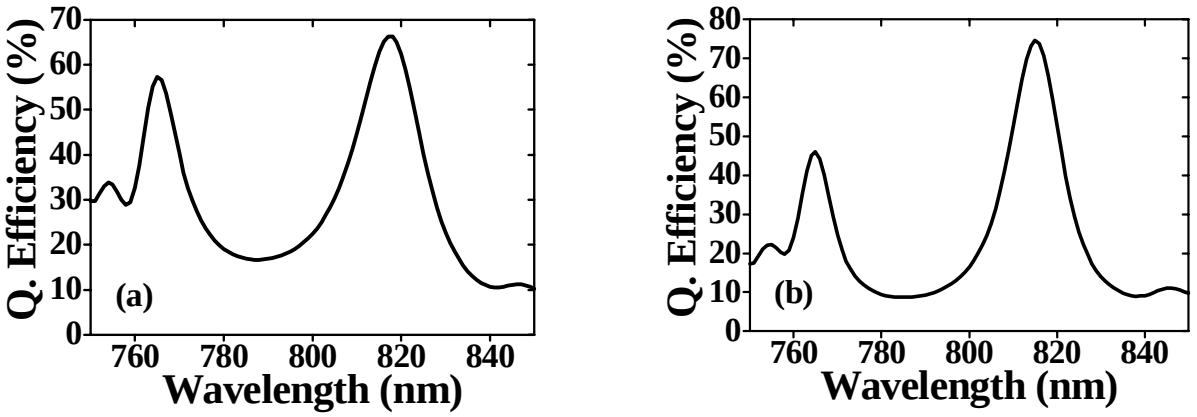

(a) (b)

Figure 3. Spectral quantum efficiency of the RCE ITO-Schottky PD (a) without top DBR (b) with 2-pair top DBR

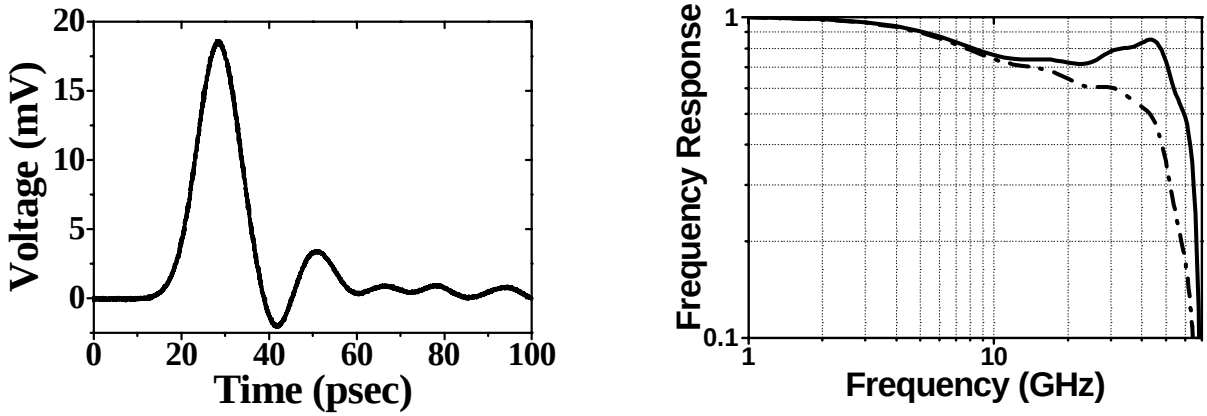

(a) (b)

Figure 4. (a) Pulse response of a 5x5μm^2 RCE ITO-Schottky PD. (b) The as-measured (dashed line) and deconvolved (solid line) frequency responses of the detectors.

Downloaded From: https://www.spiedigitallibrary.org/conference-proceedings-of-spie on 9/28/2017 Terms of Use: https://spiedigitallibrary.spie.org/ss/TermsOfUse.aspx

High-speed measurements were implemented by utilizing a picosecond mode-locked Ti:sapphire laser, which was tuned at the resonant wavelength of our detectors, 815 nm. The devices were illuminated by a single-mode fiber on a microwave probe station and the resulting pulses were observed on a 50-GHz sampling scope. The pulse response of the detector was observed to be bias dependent. While 12 psec FWHM was measured at zero bias, this value decreased to 11.5 psec for 2 V reverse bias voltage. The best measured data had a FWHM of 11.2 psec under a reverse bias of 4 V. Further increase of the bias voltage made the PD response slower, mainly due to the avalanche gain mechanism, which was significant for bias voltages higher than 5 V. Figure 4(a) shows the measured temporal response of a small area (5x5 μm^2) RCE ITO-Schottky PD under 4 V reverse bias. The Fourier transform of the temporal data has a 3-dB bandwidth of 43 GHz. The measured data was corrected by deconvolving the scope response. Considering a 9 psec FWHM for the 50 GHz scope, our detectors had a 3-dB bandwidth of 60 GHz. Figure 4(b) shows the as-measured and deconvolved frequency responses obtained from the fast Fourier transform (FFT) of the temporal detector response. The efficiency and bandwidth measurements of the fabricated RCE ITO-Schottky PDs resulted in a detector performance of 45 GHz BWE product.

4. INGAAS BASED PIN PHOTODETECTOR

4.1 Design and Fabrication

The epitaxial structure of the RCE p-i-n photodiode was designed using transfer-matrix-method based simulations. The layers were grown by molecular beam epitaxy on semi-insulating InP substrate. The bottom Bragg mirror (DBR) was made from quarter-wave stacks of InAlAs and $In_{0.53}Al_{0.13}Ga_{0.34}As$, designed for high reflectance at 1550 nm center wavelength. $In_{0.53}Al_{0.13}Ga_{0.34}As$ was chosen to achieve high refractive index contrast with the lower index InAlAs without having any optical absorption in the DBR region. Theoretically this DBR had a maximum reflectivity of 84% at 1550nm. All cavity layers except the 300-nm InGaAs absorption layer were transparent at the operation wavelengths. The details of the epitaxial structure are given in Table 1.

Material	Thickness (nm)	Doping (cm^{-3})
InGaAs	30	p+ 10^{19}
Graded Layer	30	p+ 10^{19}
InAlAs	210	p+ 10^{19}
InAlAs	50	n- 10^{16}
Graded Layer	30	n- 10^{16}
InGaAs	300	n- 10^{16}
Graded Layer	30	n- 10^{16}
InAlAs	60	n- 10^{16}
InAlAs	300	n+ $3x10^{18}$
InAlAs	240	None
25 Pair InAlAs/InAlGaAs DBR	25 x (121/112)	None
InP Substrate	600 μm	Semi-insulating

Table 1. Epitaxial structure of the InGaAs based photodetector

After the growth we measured the reflectivity spectrum of the wafer. The comparison between the measured and simulated reflectance data of the as-grown wafer showed that the layers had been grown 4% thicker than the original design. This shifted the center wavelength of the DBR to 1610 nm. Figure 5 shows the measurement and simulation results of reflectivity.

InAlAs and InGaAs layers were etched with a phosphoric acid based etchent (H_3PO_4:H_2O_2:H_2O). Ohmic contacts to n+ layers were formed by a phosphoric acid based etch that was followed by a self-aligned Au-Ge-Ni lift-off.

Downloaded From: https://www.spiedigitallibrary.org/conference-proceedings-of-spie on 9/28/2017 Terms of Use: https://spiedigitallibrary.spie.org/ss/TermsOfUse.aspx

The p+ ohmic contact was achieved by Au-Ti lift-off. The samples then were rapid thermal annealed at 400 ^{o}C for 1 min. We etched away all the layers down to undoped InAlAs except the active areas using the isolation mask. Then Ti-Au interconnect metal was evaporated, which formed the coplanar waveguide (CPW) transmission lines on top of the undoped layer. The next step was deposition and pattering of ~100-nm-thick Si_3N_4 layer. Besides passivation, the Si_3N_4 layer was also used as the dielectric of metal-insulator-metal bias capacitors. To reduce the parasitic capacitance, the p+ ohmic metal was connected to CPW pads by 0.7-μm-thick Ti-Au airbridge. The resulting RCE p-i-n photodiodes had breakdown voltages around 14 V and typical dark current densities were 10^{-5} A/cm^2 at -1 V bias.

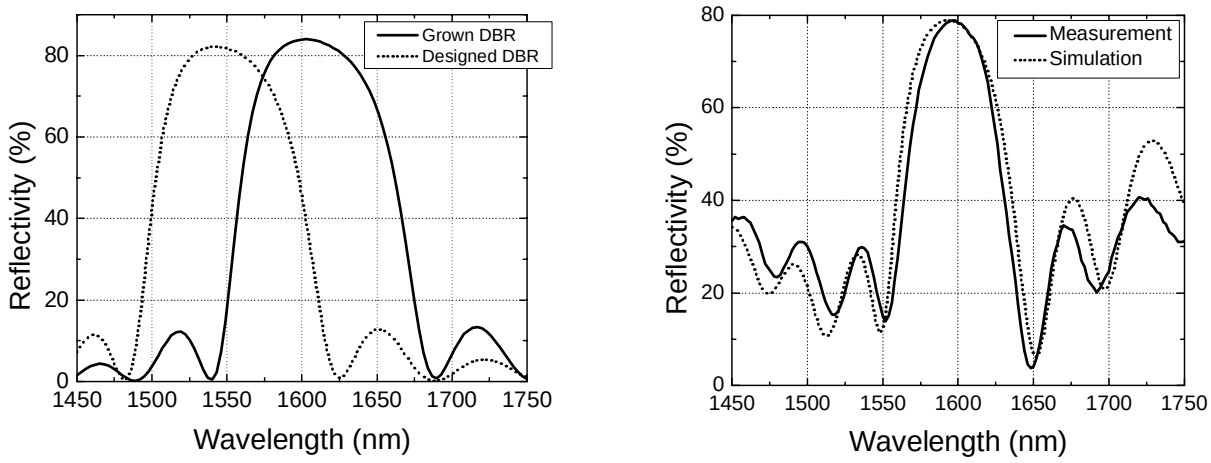

(a) (b)

Figure 5. (a) The simulation results of reflectivity of designed and grown bottom DBR mirrors. (b) Measured and simulated reflectivity results of the grown structure.

4.2 Measurements

Photoresponse measurements were carried out in the 1530-1630 nm range using a tunable laser source. The output of the laser was coupled to a single mode fiber. The light was delivered to the devices by a lightwave fiber probe, and the electrical characterization was carried out on a microwave probe station. The top p+ layers were recess etched in small steps, and the tuning of the resonance wavelength within the high reflectivity spectral region of the DBR was observed.

Figure 6(a) shows the spectral quantum efficiency measurements of a device under 5 V reverse bias obtained by consecutive recess etches. Plot 1 is the quantum efficiency after the top InGaAs layer etch, while plots 2, 3, 4, 5, 6, and 7 correspond to cumulative recess etches of 80, 105, 150, 180, 210 and 240 nm, respectively. The peak experimental quantum efficiency 30% of the as-grown sample at 1645 nm increases to 55% at 1614 nm after the first etch. The peak quantum efficiency increased up to 66% with tuning until the resonance wavelength reached 1572 nm. This increase was due to the increase of the absorption coefficient of InGaAs at shorter wavelengths. As we continued the recess etch, the peak quantum efficiency decreased due to the decrease of the reflectivity of the Bragg mirror. The resonance wavelength was tuned for a total of 47 nm (1538 – 1605 nm) while keeping the peak efficiencies above 60%. The peak efficiency was above 50% for the resonant wavelengths between 1550 and 1620 nm, corresponding to a tuning range of 70 nm.

Downloaded From: https://www.spiedigitallibrary.org/conference-proceedings-of-spie on 9/28/2017 Terms of Use: https://spiedigitallibrary.spie.org/ss/TermsOfUse.aspx

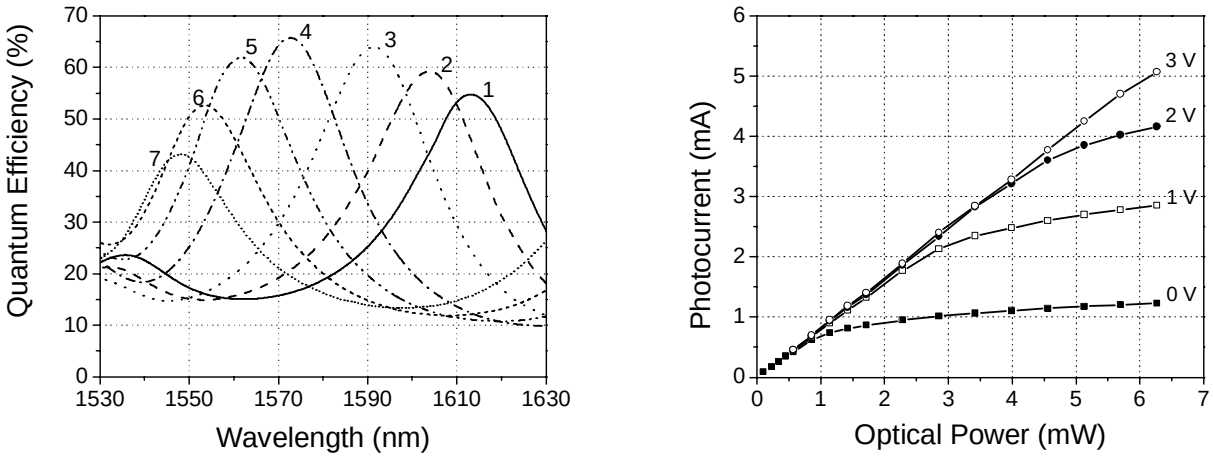

(a) (b)

Figure 6. (a) Spectral quantum efficiency measurements of the fabricated detectors after consecutive recess etches. (b) Optical input power versus photocurrent of the photodetector under various reverse biases.

The full width at half maximum (FWHM) of the devices was around 35 nm. The quantum efficiency measurements were done at 5 V reverse bias under 0.5 mW input optical power. When we increased the reverse bias beyond 3 V the active layer was fully depleted, and the quantum efficiency increased 6% with respect to zero bias. The responsivity of the PDs were also measured under various reverse biases up to 6 mW optical power, which was the maximum power that could be obtained from the laser. Figure 6(b) shows the photocurrent versus input optical power at the resonance wavelength of 1572 nm. Under 3 V and higher reverse biases, the PDs had a linear photoresponse up to 6 mW optical power. At 6 mW optical power, the device exhibited a 5 mA photocurrent. The saturation was mainly due to the electric field screening caused by photo-generated carriers[33].

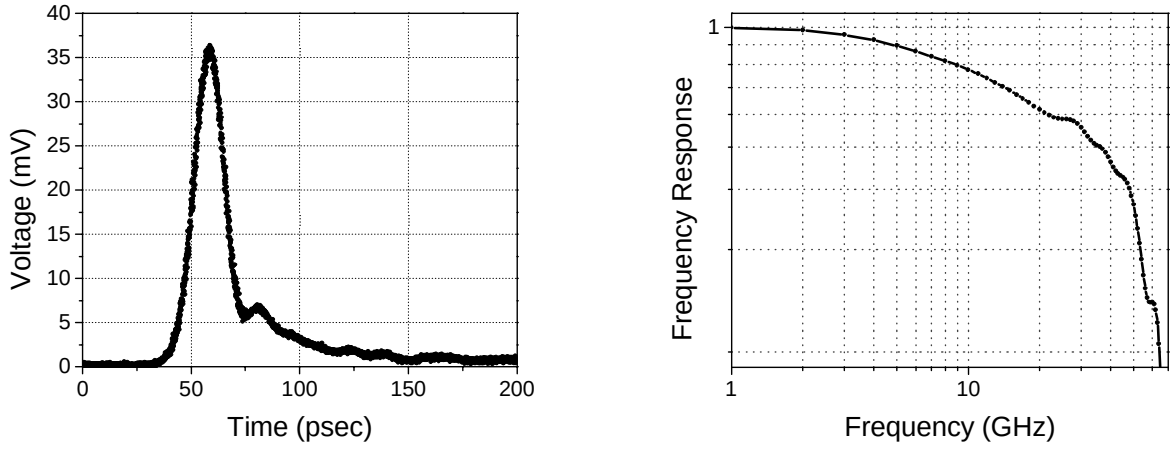

(a) (b)

Figure 7. (a) Temporal response of the photodetector with a 16 psec full width at half maximum. (b) The deconvolved frequency response obtained from the fast Fourier transform of the temporal dedetector response.

Downloaded From: https://www.spiedigitallibrary.org/conference-proceedings-of-spie on 9/28/2017 Terms of Use: https://spiedigitallibrary.spie.org/ss/TermsOfUse.aspx

High-speed measurements were made with a picosecond fiber laser operating at 1550 nm. The 1 ps FWHM optical pulses from the laser were coupled to the active area of the p-i-n photodiodes by means of a fiber probe. At zero bias, the response of the photodetectors had a long tail due to the diffusion of the carriers in the active layers. Measurements were done under bias to deplete the active layer completely and to get rid of the diffusion tail. Above 3 V reverse bias, we got a Gaussian response with a short tail. Figure 7(a) shows the temporal response of a small area (5 x 5 μm^2) photodetector measured at 7 V bias by a 50 GHz sampling scope. The photodiode output had a 16 ps FWHM. The measured data was corrected by deconvolving the effect of the 40 GHz bias-tee. After the deconvolution, the device had a 3-dB bandwidth of 31 GHz. Larger area devices (80 μm^2) also showed similar responses, which showed that the temporal response was limited by the transport of the photogenerated carriers. The measured bandwidth is lower than the theoretically predicted 3-dB bandwidth of 55 GHz [25]. Although grading layers have been implemented to avoid carrier trapping, our measurement data shows that the device performance is still limited by the carrier trapping. In our devices, we used a digital grading that consisted of InP lattice matched InGaAs/InAlAs layers. A linear grading may further improve the device performance.

5. CONCLUSION

We reviewed our recent work on ultrafast high-efficiency resonant cavity enhanced photodetectors. Using a microwave compatible planar fabrication process, we have designed and fabricated GaAs and InGaAs based RCE PDs. For RCE Schottky type photodiodes, we have improved the 25 GHz BWE performance to 45 GHz BWE by using a transparent ITO-Schottky layer and a dielectric top Bragg mirror instead of semitransparent Au-Schottky metal. For the RCE p-i-n photodetector, we have achieved 20 GHz BWE. The detectors had linear and high output current up to 5 mA under 3 V bias. To the best of our knowledge, these BWE values correspond to the highest detector performances reported for vertically illuminated p-i-n and Schottky photodiodes.

6. ACKNOWLEDGEMENTS

This work was supported by NATO Grant No. SfP971970, National Science Foundation Grant No. INT-9906220, Turkish Department of Defense Grant No. KOBRA-001.

REFERENCES

[1] J. E. Bowers and Y. G. Wey in *Handbook of Optics*, chap. 17, McGraw-Hill, New York, 1995.

[2] K. Kato, "Ultrawide-band/high-frequency photodetectors," *IEEE Trans. Microwave Theory Tech.* **47**, pp. 1265-1281, 1998.

[3] H. Ito, T. Furuta, Y. Hirato, T. Ishibashi, A. Hirata, T. Nagatsuma, H. Matsuo, T. Noguchi, and M. Ishiguro, "Photonic millimeter-wave emission at 300 GHz using an antenna-integrated uni-traveling-carrier photodiode," *Electron. Lett.*, **38**, pp. 989-990, 2002.

[4] S. Y. Wang, and D. M. Bloom, "100 GHz bandwidth planar GaAs Schottky photodiode," *Electron. Lett.* **19**, pp. 554-555, 1983.

[5] E. Özbay, K. D. Li, and D. M. Bloom, "2.0 psec, 150 GHz GaAs Monolithic Photodiode and All-Electronic Sampler", *IEEE Photon. Technol. Lett.* **3**, pp. 570-572, 1991.

[6] K. D. Li, A. S. Hou, E. Özbay, and D. M. Bloom, "2.0 psec GaAs photodiode optoelectronic circuit for correlation applications," *Appl. Phys. Lett.* **61**, pp. 3104-3106, 1992.

Downloaded From: https://www.spiedigitallibrary.org/conference-proceedings-of-spie on 9/28/2017 Terms of Use: https://spiedigitallibrary.spie.org/ss/TermsOfUse.aspx

[7] Y. G. Wey, M. Kamegawa, A. Mar, K. J. Williams, K. Giboney, D. L. Crawford, J. E. Bowers, and M. J. Rodwell, *J. Lightwave Technol.* **13**, pp. 1490-1494, 1995.

[8] Y. G. Wey, K. S. Giboney, J.E. Bowers, M. J. W. Rodwell, P. Silvestre, P. Thiagarajan, and G.Y. Robinson, IEEE Photon. Technol. Lett. **5**, pp. 1310-1312, 1993.

[9] Jin-Wei Shi, Kian-Giap Gan, Yi-Jen Chiu, Chi-Kuang Sun, Ying-Jay Yang, and John E. Bowers, "Metal-semiconductor-metal traveling-wave photodetectors", *IEEE Photon. Technol. Lett.*, **16**, pp. 623-625, 2001.

[10] I-Hsing Tan, Chi-Kuang Sun, Kirk S. Giboney, John E. Bowers, Evelyn L. Hu, B. I. Miller, and R. J. Capik, "120-GHz long-wavelength low-capacitance photodetector with an air-bridge coplanar metal waveguide", *IEEE Photon. Technol. Lett.*, **7**, pp. 1477-1479, 1995.

[11] E. Drödge, E. H. Böttcher, St. Kollakowski, A. Strittmatter, D. Bimberg, O. Riemann, and R. Steingrüber, "78 GHz InGaAs MSM photodetector", *Electron. Lett.*, **34**, pp. 2241-2243, 1998.

[12] G. S. Kinsey, C. C. Hansing, A. L. Holmes, Jr., B. G. Streetman, J. C. Campbell, and A. G. Dentai, "Waveguide $In_{0.53}Ga_{0.47}As$-$In_{0.52}Al_{0.48}As$ Avalanche Photodiode", *IEEE Photon. Technol. Lett.*, **12**, pp. 416-418, 2000.

[13] Sanjeev Murthy, Thomas Jung, Tai Chau, Ming C. Wu, Deborah L. Sivco, and Alfred Y. Cho, "A novel monolithic distributed traveling-wave photodetector with parallel optical feed", *IEEE Photon. Technol. Lett.*, **12**, pp. 681-683, 2000.

[14] M. S. Unlu and S. Strite, "Resonant cavity enhanced (RCE) photonic devices," *J. Appl. Phys. Rev.*, vol. 78, no. 2, pp. 607-639, 1995.

[15] K. Kishino, M. S. Ünlü, J. I. Chyi, J. Reed, L. Arsenault, and H. Morkoç, "Resonant cavity-enhanced (RCE) photodetectors," *IEEE J. Quantum Electron.,* 27, pp. 2025-2031, 1991.

[16] I. H. Tan, E. L. Hu, J. E. Bowers, and B. I. Miller, "Modeling and performance of wafer-fused resonant-cavity enhanced photodetectors," *IEEE J. Quantum Electron.*, **31**, pp. 1863-1869, 1995.

[17] M. S. Unlu, K. Kishino, J. I. Chyi, L. Arsenault, J. Reed, and H. Morkoc, "Wavelength demultiplexing heterojunction phototransistor", *Electron. Lett.*, **26**, pp. 1857-1858, 1990.

[18] S. S. Murtaza, I. H. Tan, J. E. Bowers, E. H. Lu, K. A. Anselm, M. R. Islam, R. V. Chelakara, R. D. Dupuis, B. G. Streetman, and J. C. Campbell, "High-finesse resonant-cavity photodetectors with an adjustable resonance frequency", *J. Lightwave Technol.*, **14**, pp. 1081–1089, 1996.

[19] Hui Nie, K. A. Anselm, C. Hu, S. S. Murtaza, B. G. Streetman, and J. C. Campbell, "High-speed resonant-cavity separate absorption and multiplication avalanche photodiodes with 130 GHz gain-bandwidth product", *Appl. Phys. Lett.*, **70**, pp. 161-163, 1997.

[20] E. Ozbay, I. Kimukin, N. Biyikli, O. Aytur, M. Gokkavas, G. Ulu, M. S. Unlu, R. P. Mirin, K. A. Bertness, and D. H. Christensen, "High-speed >90% quantum efficiency p-i-n photodiodes with a resonance wavelength adjustable in the 795-835 nm range," *Appl. Phys. Lett.*, **74**, pp. 1072-1074, 1999.

[21] M. Gokkavas, O. Dosunmu, M. S. Unlu, G. Ulu, R. P. Mirin, D. H. Christensen, and E. Ozbay, "High-Speed High-Efficiency Large-Area Resonant Cavity Enhanced p-i-n Photodiodes for Multimode Fiber Communications," *IEEE Photon. Technol. Lett.*, **13**, pp. 1205-1207, 2001.

[22] X. Sun, J. Hsu, X. G. Zheng, J. C. Campbell, and A. L. Holmes, "GaAsSb resonant-cavity-enhanced photodetector operating ay 1.3 μm," *IEEE Photon. Technol. Lett.*, **14**, pp. 681-683, 2002.

Downloaded From: https://www.spiedigitallibrary.org/conference-proceedings-of-spie on 9/28/2017 Terms of Use: https://spiedigitallibrary.spie.org/ss/TermsOfUse.aspx

[23] E. Ozbay, I. Kimukin and N. Biyikli, "Ultrafast & Highly Efficient Resonant Cavity Enhanced Photodiodes," *Materials Science Forum*, **384-385**, pp. 241-248, 2002.

[24] Y. H. Zhang, H. T. Luo, and W. Z. Shen, "Demonstration of bottom mirrors for resonant-cavity-enhanced GaAs homojunction far-infrared detectors," *Appl. Phys. Lett.*, **82**, pp. 1129-1131, 2003.

[25] C. C. Barron, C. J. Mahon, B. J. Thibeault, G. Wang, W. Jiang, L. A. Coldren, and J. E. Bowers, "Resonant-cavity-enhanced pin photodetector with 17 GHz bandwidth efficiency product", *Electron. Lett.*, **30**, pp.1796-1797, 1994.

[26] P. Yuan, O. Baklenov, H. Nie, A. L. Holmes, B. G. Streetman, and J. C. Campbell, "High-Speed and Low-Noise Avalanche PhotodiodeOperating at 1.06 μm," *IEEE J. Select. Topics in Quantum Electron.*, 6, pp. 422-424, 2000.

[27] C. Lennox, H. Nie, P. Yuan, G. Kinsey, A. L. Holmes, B. G. Streetman, and J. C. Campbell, "Resonant-cavity InGaAs-InAlAs avalanche photodiodes with gain-bandwidth product of 290 GHz," *IEEE Photon. Technol. Lett.*, **11**, pp. 1162-1164, 1999.

[28] M. S. Unlu, M. Gokkavas, B. M. Onat, E. Ata, E. Ozbay, R. P. Mirin, K. J. Knopp, K. A. Bertness, and D. H. Christensen, "High badwidth-efficiency resonant cavity enhanced Schottky photodiodes for 800-850 nm wavelength operation," *Appl. Phys. Lett.*, **72**, pp. 2727-2729, 1998.

[29] N. Biyikli, I. Kimukin, O. Aytür, M. Gökkavas, M. S. Ünlü, and E. Ozbay, "45-GHz bandwidth-efficiency resonant-efficiency-enhanced ITO-schottky photodiodes", *IEEE Photon. Technol. Lett.*, **13**, pp. 705-707, 2001.

[30] I. Kimukin, N. Biyikli, B. Butun, O. Aytur, S. Ünlü, and E. Ozbay, " InGaAs Based High Performance p-i-n Photodiodes," *IEEE Photon. Tech. Lett.*, **14**, pp. 366-368, 2002.

[31] D. G. Parker, P. G. Say, and A. M. Hansom, "110-GHz high-efficiency photodiodes fabricated from indium–tin–oxide/GaAs," Electron. Lett., 23, pp. 527-528, 1987.

[32] W. A. Wohlmuth, J.-W. Seo, P. Fay, C. Caneau, and I. Adesida, "A high-speed ITO-InAlAs-InGaAs Schottky-barrier photodetector ," *IEEE Photon. Technol. Lett.*, **9**, pp. 1388-1390, 1997.

[33] L. Y. Lin, M. C. Wu, T. Itoh, T. A. Vang, R. E. Muller, D. L. Sivco, and A. Y. Cho, "High-power high-speed photodetectors-Design, analysis, and experimental demonstration", *IEEE Trans. Microwave Theory. Tech.*, **45**, pp. 1320-1331, 1997.

Downloaded From: https://www.spiedigitallibrary.org/conference-proceedings-of-spie on 9/28/2017 Terms of Use: https://spiedigitallibrary.spie.org/ss/TermsOfUse.aspx